

New Insights into AA7085 Environmentally Assisted Cracking through High Resolution Fractography

I. Field[1], J. Rogers[2], & N. Tugwell[1]

[1]Defence Science and Technology Group, Australian Department of Defence, 506 Lorimer Street, Fishermans Bend, Melbourne, Vic, 3027, Australia.
[2]Royal Melbourne Institute of Technology, 124 La Trobe Street, Melbourne, Vic, 3000, Australia.

Abstract

Environmentally assisted cracking (EAC) in the new generation aluminium alloy (AA) 7085 has recently become a critical area of research in aircraft sustainment due to its inclusion in modern aircraft structures and the recent acknowledgement of its EAC susceptibility. This assessment was done by the European Union Aviation Safety Agency, where they found that industry standard tests were unable to identify AA7085's true vulnerability to all forms of EAC. The reason for this appears to be linked to AA7085's susceptibility to cracking at grain boundaries in hot and humid environments, regardless of the chloride content of that environment. However, despite the recent literature focusing on characterising this material, little direct observation of the EAC crack surfaces at high resolution has been published. This direct observation may lead to new insights into the mechanisms behind this EAC growth. Additionally, it can provide information on key EAC features that may be useful in interpreting how these cracks grow, which is crucial for future forensic analysis of EAC cracks found in aircraft structures. This paper provides a detailed summary of high resolution fractographic features associated with EAC, and an interpretation of the clues these features provide as to the growth mechanisms and sequence.

Keywords: EAC, AA7085, Fractography, Cracking, FEGSEM.

1. Introduction

Aluminium alloy (AA) 7085 is a new generation high strength aluminium alloy used in modern civilian and military aircraft [1]. It is an attractive material to manufacturers due to its ability to be used in manufacturing large die forged structures up to 305 mm (12 in) thick [2]. This is due to its comparatively higher purity and improved quench sensitivity compared to older generation 7xxx series aluminium alloys [3]. It was registered with the Aluminum Association in 2002, and is one of many new generation 7xxx series alloys designed to cater for the trend in modern aircraft manufacturing towards high speed machining of large components [4]. This allows thick near-net die forgings of complex structures to be produced that require significantly less machining compared to equivalent structure from plate. One natural consequence of this material being used for thick unitised aerospace structures is that they tend to be the primary load carrying components within aircraft [5]. As such, many of these parts are deemed fracture critical, whereby their failure could lead to the loss of the aircraft. This means that any potential susceptibility the material may have towards a failure mode must be carefully analysed and understood to mitigate and manage the risks it poses to aircraft fleets.

One such susceptibility became evident in 2018 when the European Union Aviation Safety Agency (EASA) published a safety information bulletin (SIB) on environmentally assisted cracking (EAC) in multiple new generation aluminium alloys, including AA7085 [6]. This is despite the industry standard ASTM G44 [7] alternate immersion tests used to assess a material's susceptibility to stress corrosion

https://doi.org/10.71945/icas2026_0234

cracking (SCC) being successfully completed and passed for this alloy [3]. Airbus provided a likely reason for this discrepancy, where they showed that the relative time to failure of AA7085 compared to AA7075-T6 would reverse when subject to a hot and humid environment compared to the saltwater environment of ASTM G44 [8]. This demonstrated a particular susceptibility of the new generation aluminium alloys to a hot and humid environment, regardless of its chloride content, and is thought to be primarily due to hydrogen embrittlement along grain boundaries [6].

It should be noted that there has long been discussion in the literature as to the relative roles of hydrogen embrittlement versus anodic dissolution of grain boundary precipitates (GBPs) or the aluminium matrix in SCC [9-13]. This is despite some researchers appearing to align with the EASA SIB [6], designating EAC as a hydrogen embrittlement phenomena and SCC as an anodic dissolution phenomena [14, 15]. However, many others have contradicted the SIB, claiming that SCC also grows through a hydrogen embrittlement process [9-11, 16-20], resulting in no clear distinction between EAC and SCC. To complicate matters further, there are a wide range of terms used to describe this phenomena that are not always distinguished clearly from each other. For example, some research uses the term hydrogen EAC (HEAC [4] or H-EAC [15]) and others use the term environmentally induced cracking (EIC) [21] (or H-EIC [22]). Whilst the precise name chosen may not be critical, confusion on this matter can have the indirect effect of obscuring the vast amount of research already completed on this topic under different names. As such, each of the above terms can be thought of synonymously for this paper, similar to what other researchers have done [4, 23]. This is because all the terms describe the cracking of a susceptible material when exposed to a combination of environmental and loading conditions. Differentiating between the various terms based on growth mechanisms is a highly subjective task when there is still debate in the literature as to what the mechanisms truly are.

Despite the above, there appears to be a difference in rate controlling mechanisms for older generation aluminium alloys compared to new generation alloys, as their growth behaviors can reverse under saltwater versus hot and humid conditions [8]. It has been suggested that this is due to differences in initiation time versus growth rate for these materials [4]. Whereby newer, cleaner, alloys may take longer to initiate EAC, but could produce faster overall EAC growth if its microstructure exhibits longer continuous grains. It has even been suggested that different mechanisms may be responsible for each stage, where anodic dissolution could control the initiation phase and hydrogen embrittlement the crack growth phase [11]. There are a range of techniques that can be used to assess the relative importance of these mechanisms, such as utilising hydrogen pre-charging [14], as well as analytical methods including nuclear reaction analysis, focused ion beam secondary ion mass spectroscopy, and thermal desorption spectroscopy [18]. However, many of these methods have not yet been used on AA7085, and can require highly specialised equipment that not all laboratories may have access to.

In contrast to the above techniques, one important and widely accessible tool for interpreting EAC is that of direct fractographic observation, as has historically been utilised for fatigue cracks [24, 25]. This can go beyond just categorising the cracks as EAC, and should rather employ all available methods to obtain as much information as possible about crack initiation, growth, and final failure (if present), as well as searching for clues as to the growth mechanisms. Such analysis is best conducted in high resolution microscopes, such as a field emission gun scanning electron microscope (FEGSEM), and care must be taken to ensure the effects of the various imaging settings are understood, such as will be discussed in section 3.1.

Another feature commonly associated with EAC is that of crack arrest marks (CAMs). These CAMs are generally thought to be regions of increased oxide buildup that are associated with the crack tip location throughout its growth [4]. It has, however, also been suggested that the CAMs are associated with crack tip blunting [20]. The literature states that the spacing of these CAMs is typically between 100 nm to 500 nm and that it is largely insensitive to the stress intensity factor [11,

16, 26]. This infers that when an EAC crack grows faster, the amount of time between each increment of growth reduces, rather than the spacing increasing. The appearance of CAMs is thought to indicate that EAC growth occurs intermittently [17]. This predicts the formation of a zone of reduced toughness head of the crack tip, driven by anodic dissolution and/or hydrogen embrittlement. Once a critical toughness is achieved, the crack would jump forwards a distance equal to the CAM spacing, at which point it would arrest and the process would repeat itself. It is likely that close direct analysis of these CAMs could provide additional clues as to the mechanisms of growth, where evidence of increased oxide buildup or dissolution of GBPs could be sought out.

It is also of use to develop a robust method to track EAC cracks back to their initiation locations, as unambiguous identification of these initiating features may provide clues as to the root cause of the EAC. One feature that can be used is that of the aforementioned CAMs, as they are known to align with the crack tip, and are thus perpendicular to the direction of growth. However, these CAMs are often only found in limited locations across the cracks [14, 15], meaning that they cannot in isolation be relied on to trace the crack back to its origin. As such, other features should be sought that can be used in a supportive manner. One example is that of river patterns. These are often utilised when analysing fatigue cracks and are step-height changes in the crack surface that connect two growth planes together [27-29]. They are aligned approximately parallel with the local growth direction and can be used to trace fatigue cracks back to their origins. However, this technique does not appear to be used in the literature on EAC cracks, necessitating further analysis.

The observations provided here explore the range of fractographic features that can be observed in conjunction with the impact that image settings can have on the observability of these features. With the increased interest in EAC for new generation aluminium alloys, mechanistic description of these processes and features are important to ensure that the cracks can be correctly interpreted under both test and real-world conditions.

2. Experimental Method

A range of tests were conducted on coupons cut from an AA7085-T7452 forging. These coupons had nominal dimensions of 35×35×5 mm with a centre hole machined of varying diameters from 4 mm to 6.3 mm. Each of these coupons were anodised in accordance with MIL-A-8625 type 1C, class 1 sulphuric acid process prior to having their holes machined. This was in order to ensure the surface condition was representative of aircraft [30]. Each of the fastener holes were exposed to a solution of 0.05 M/L potassium persulfate and 0.033 M/L aluminium chloride (PP+AC), topped up with deionized water, for different amounts of time to produce rapid intergranular corrosion (IGC) from which EAC could initiate and grow. This was to shorten the total test times, as early EAC initiation and growth can consume a significant portion of this [31]. Finally, hi-lok fasteners of varying interference levels were installed to impart a sustained tensile stress field around the hole necessary for EAC growth [6]. The range of conditions tested are shown in Table 1.

Table 1 – The range of different hole sizes, exposure times, and interference levels used in the IFF EAC tests. The coupon with the test conditions in bold was the focus for fractographic examination and is considered representative of all the analysed coupons.

Nominal hole size	PP+AC exposure time (hr)	Interference level
1/4 in.	24 hours	0.50%
1/4 in.	24 hours	2.00%
1/4 in.	8 hours	0.50%
1/4 in.	8 hours	2.00%
1/4 in.	2 hours	0.50%
3/16 in.	24 hours	1.00%
3/16 in.	8 hours	0.50%

3/16 in.	8 hours	1.00%
3/16 in.	2 hours	1.00%
3/16 in.	2 hours	2.00%
5/32 in.	**24 hours**	**1.50%**
5/32 in.	8 hours	1.00%
5/32 in.	8 hours	1.50%
5/32 in.	2 hours	1.00%
5/32 in.	2 hours	1.50%

The coupons were then left in an environmental chamber for 52 to 62 days, and exposed to 70°C and 85% RH air in line with the testing conditions recommended by the EASA SIB [6]. At the end of their exposure period there was evidence that many of the coupons had grown cracks in the longitudinal grain direction away from the fastener holes, as shown in Figure 1. Each of the coupons were cut through the hole perpendicular to the cracking direction, and then each half was stressed in three-point bending to open the cracks. These cracks were then analysed using optical microscopes and a FEGSEM.

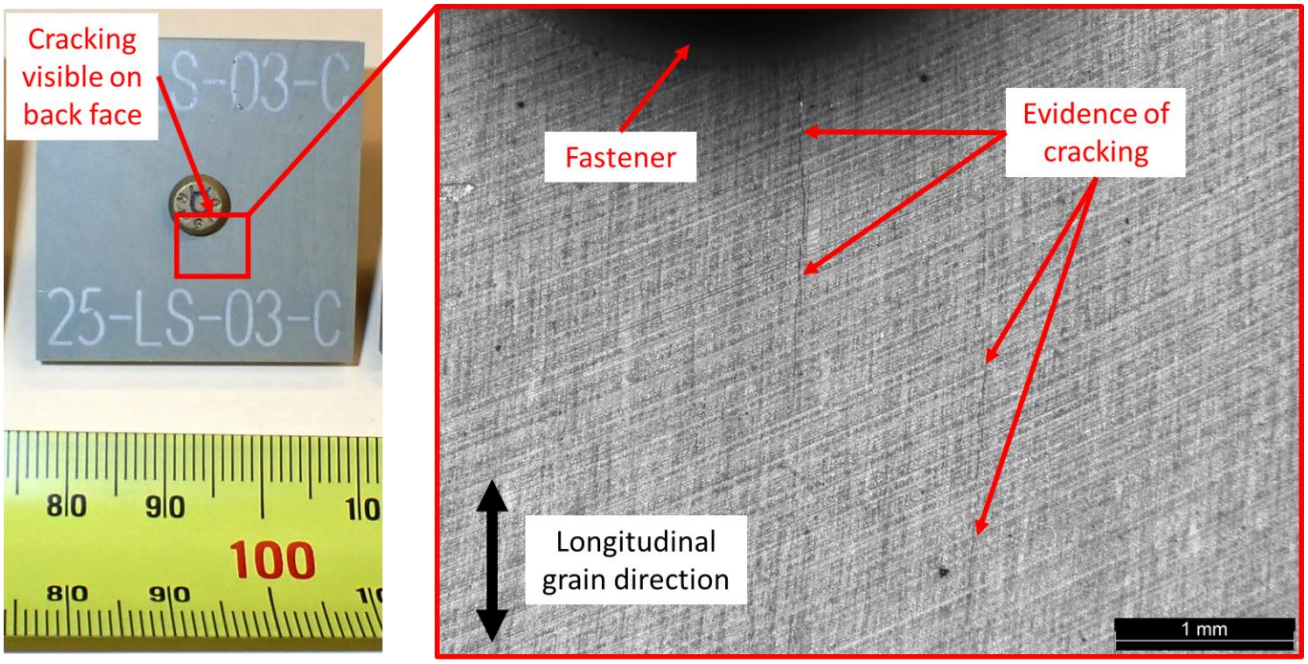


Figure 1 – An image showing the analysed coupon with the fastener installed, as well as an optical image showing some of the surface cracks that had grown during the testing period.

Whilst a wide range of coupons were tested with different PP+AC exposure times and interference fit levels as part of this program, only one coupon will be analysed in detail here. The features found were consistent across the coupons, so the observations for this coupon are representative of the wider group.

Finally, real world findings of EAC cracks were analysed to assess if, and to what extent, cracks grown in coupons in a lab environment are representative. This allowed the fractographic features of the coupon tests and the aircraft crack to be catalogued, and any differences to be noted. This is of particular use when analysing features found on an aircraft crack, where the precise conditions it was exposed to are not known. It is thought that the comparison of the aircraft crack and coupon tests with known conditions may provide insight into the aircraft's operational environment.

3. Results and Discussion

One half of the analysed coupon crack is shown in Figure 2. These images were taken using an

optical microscope. A number of key features are identifiable. The crack tip of the EAC is at the interface between surface features associated with EAC and tensile overload. Pitting associated with exposure to the PP+AC solution is at the bore of the hole. It was observed in other tests conducted by the authors that a small level of intergranular growth would extend beyond the PP+AC pits. This intergranular growth would likely allow the EAC to rapidly initiate and continue growing. Finally, potential river patterns can be seen on the surface, aligning such that they indicate the main site of crack initiation was near the corner of the coupon. This supports the expected initiation location based on the known dependence of EAC cracks in AA7085-T7452 on the stress intensity factor during early growth [4, 11]. Closer examination revealed that the primary initiation location was likely the PP+AC pit near the corner, as marked in Figure 2. However, additional evidence will be sought and analysed below, assessing the initiation location and mechanisms that may have been responsible for the EAC growth.

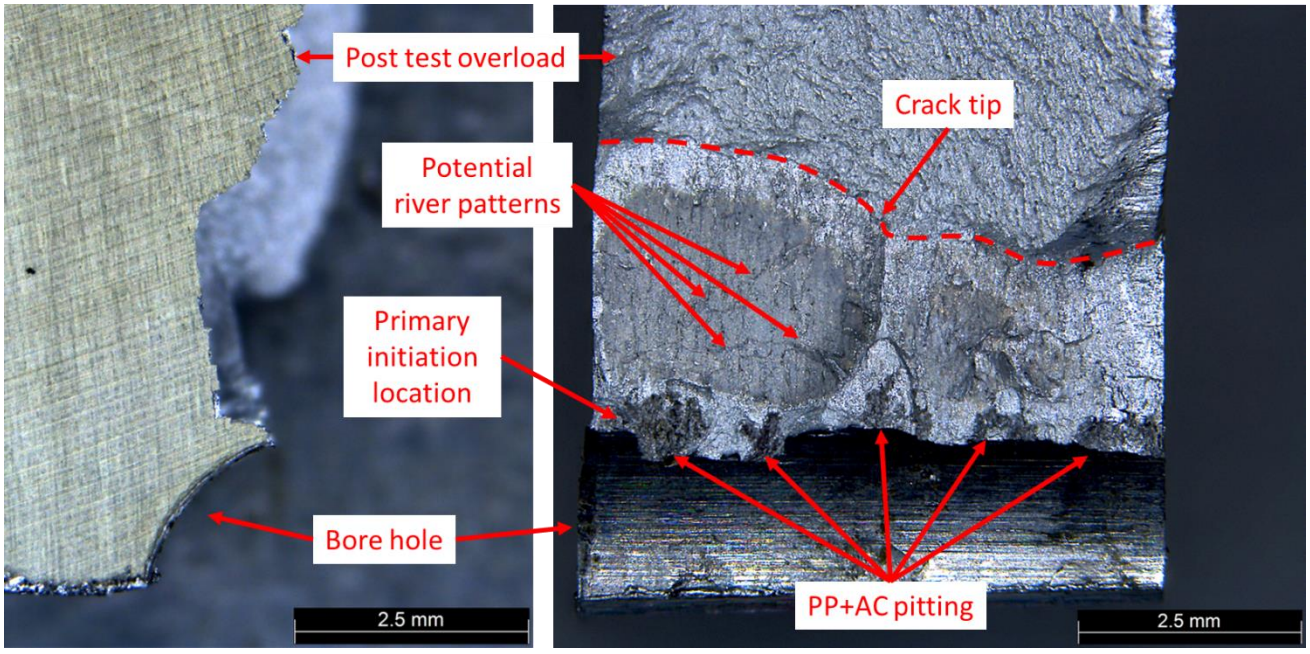


Figure 2 - One half of the analysed crack. A number of features can be identified, such as the crack tip, potential river patterns, and pitting in the bore hole associated with the PP+AC solution. The primary initiation location has also been marked.

3.1 Imaging Settings

Prior to any detailed analysis of these cracks, it is first important to understand the effect of different imaging settings on the observed features. This is particularly necessary when using a FEGSEM, as both the choice of detector and acceleration voltage can drastically change the appearance of the crack surface. The effects of this are important to recognise, particularly when comparing any features to reference images, such as those provided in the EASA SIB [6].

One setting of importance is that of acceleration voltage, whereby an increase in acceleration voltage also increases the velocity (and kinetic energy) of the imaging electrons. This increase in velocity can improve the signal-to-noise ratio of the image, but also causes the electrons to penetrate deeper into the target material, potentially imaging through features of interest on the surface. An example of this is shown in Figure 3 from a location on the analysed coupon where CAMs were present. Both images were taken using the same detector, but the left image used an acceleration voltage of 5 kV, while the right image used 20 kV. It is evident that far more surface detail can be seen with the lower acceleration voltage, including the CAMs being more easily identifiable. This is an important factor when considering previous statement in the literature about CAMs only being visible in specific regions of EAC cracks [14, 15]. In both the referenced papers [14, 15] acceleration voltages of 3-5 kV were used, giving confidence that many of the CAMs were likely identified. However, as will be shown in section 3.3, sometimes acceleration voltages as low as 0.5 kV are necessary to identify CAMs.

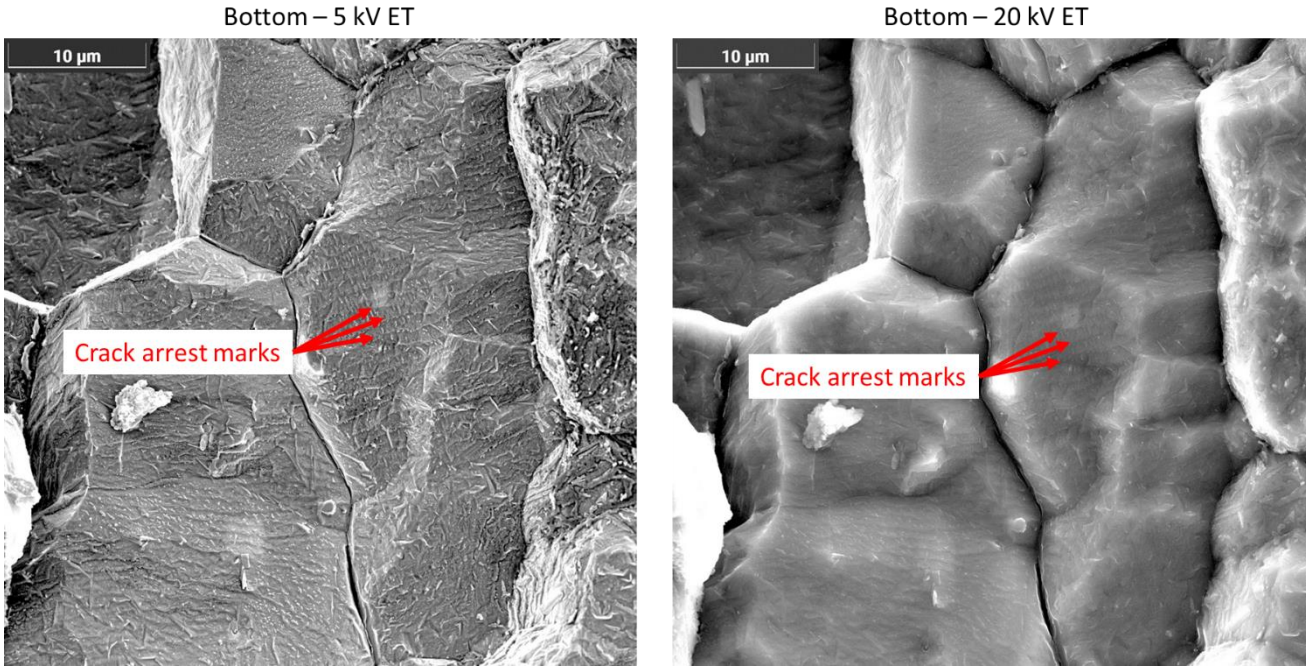


Figure 3 – Two images of the same location on an EAC crack surface using different electron acceleration voltages (left = 5 kV, right = 20 kV). Surface features, such as CAMs, can be seen more easily in the left image compared to the right image.

Another important setting is the choice of detector, with the most commonly used being the Everhart-Thornley (ET) and backscatter electron (BSE) detectors. The ET detector primarily images electrons released from near the surface of the material [27, 32] whereas the BSE detector can provide contrast related to the composition of the imaged materials [25]. As such, the ET detector usually gives increased surface feature detail, and is the detector used in Figure 3, while the BSE detector can better identify features such as corrosion product and thick oxide layers. For example, the images in Figure 4 are of the identical location using the same acceleration voltage, but the left image utilises the ET detector while the right image utilises the BSE detector. As expected, more surface detail can be identified with the ET detector, whereas the darkness on the BSE image is indicative of corrosion product. This was confirmed used energy dispersive spectroscopy (EDS), where the dark covering was found to be oxygen rich, as is expected for corrosion product. It was also far thicker than the standard natural oxide layer that aluminium has, which is typically only a few nanometers thick [33].

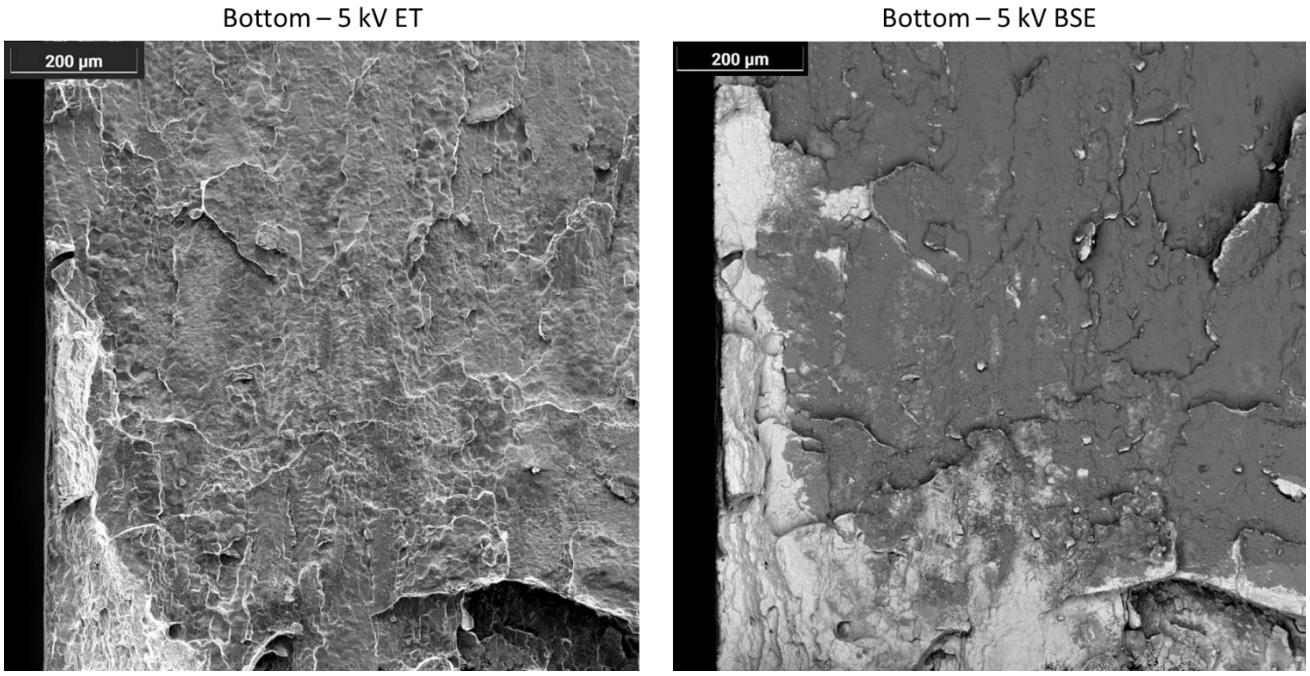


Figure 4 – Two images of identical locations on an EAC crack surface using different detectors. The ET detector (left) is better at imaging topographical features, while the BSE detector (right) is better at identifying corrosion product.

Considering the influence of both the acceleration voltage and detector choice, it is worth noting that the reference EAC images provided in the EASA SIB [6] were likely done using an ET detector and a high acceleration voltage. This is based on the authors' assessment, as the acceleration voltage and detector were not explicitly stated in the SIB. A high acceleration voltage and use of an ET detector would mean that thin layers of corrosion product would not have been detectable. This may be one reason why it categorised EAC as being a corrosion free process. The SIB also provides no guidance on the settings to be used to validate the presence or lack of corrosion product. Without standardised image settings it is very difficult to compare different EAC occurrences and identify that they may be occurring under the same mechanism or similar conditions.

Throughout the rest of this paper, unless otherwise stated, the acceleration voltage used for each image was 5 kV, as this provided a good trade-off between surface detail and signal-to-noise ratio. The detector used for each image has also been indicated in each of the figures.

3.2 General EAC Appearance

With the influence of acceleration voltage established it is worth considering whether the coupon EAC cracks truly represent those seen in real-world fleets, as well as identifying other key features associated with their growth mechanisms. This is important as it dictates whether or not observations from coupon tests may be used to inform understanding of crack behavior in the fleet. Some of the features that are considered include the intergranular nature of EAC cracking, the appearance of secondary cracks, and the distribution of corrosion product across the surface.

Figure 5 compares the near tip region of an aircraft AA7085-T7452 EAC crack with that of the coupon. The crack tips are identified by the red dashed lines, with the fracture surfaces beyond the tips being characterised by ductile overload associated with the fragments being broken open post-testing or post-excision. Both images were taken at comparable magnifications, with similar key features observable. Firstly, the growth was intergranular for both cracks, as is evident by the facetted appearance that allows the surfaces of individual material grains to be identified. Additionally, a comparable quantity of corrosion product can be seen on both cracks. This corrosion product obscures some regions of the crack surfaces, but is still sparse enough that many grains can be identified. As such, the similarity between coupon EAC and fleet crack appearance suggests that observations from coupon tests may be informative of fleet crack growth behaviour.

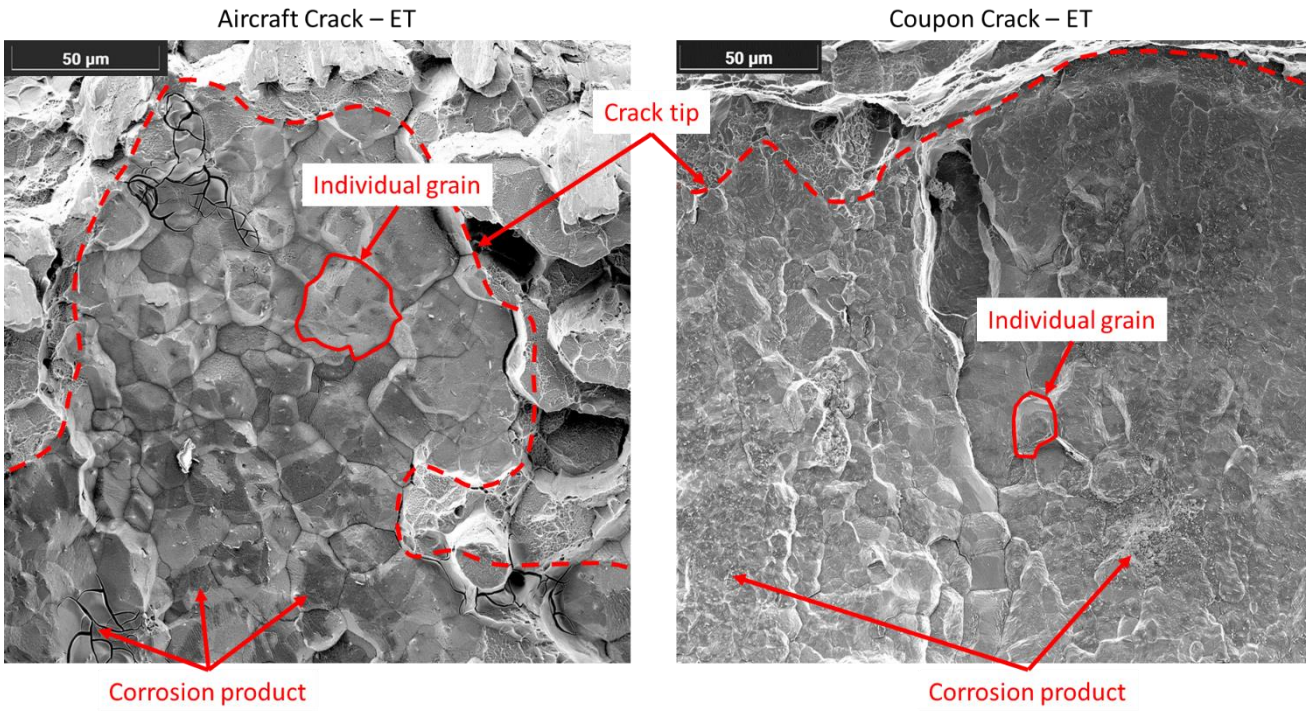


Figure 5 – Comparative images of an aircraft EAC crack versus a coupon EAC crack showing similar features.

Another feature that is associated with EAC growth, which was observed on both coupon and aircraft cracks, is that of secondary cracking. This secondary cracking is due to growth on two overlapping planes. When the crack is broken open post-testing these regions with secondary cracks can often be bent upwards from the surface, providing features akin to woodchips. An example of this is shown in Figure 6, where the left image provides an indication of some of the more prominent 'woodchip' features, while the right image is a magnified view of one of them showing how the EAC growth crosses over on the two planes. Ductile tearing can be seen on the tip of the 'woodchip' that indicates that the region was broken open during the post-test overload, bending the feature upwards in the process. This ductile tearing will be considered more closely later in this paper when analysing whether these features can be considered adjacent to the river patterns observed in fatigue.

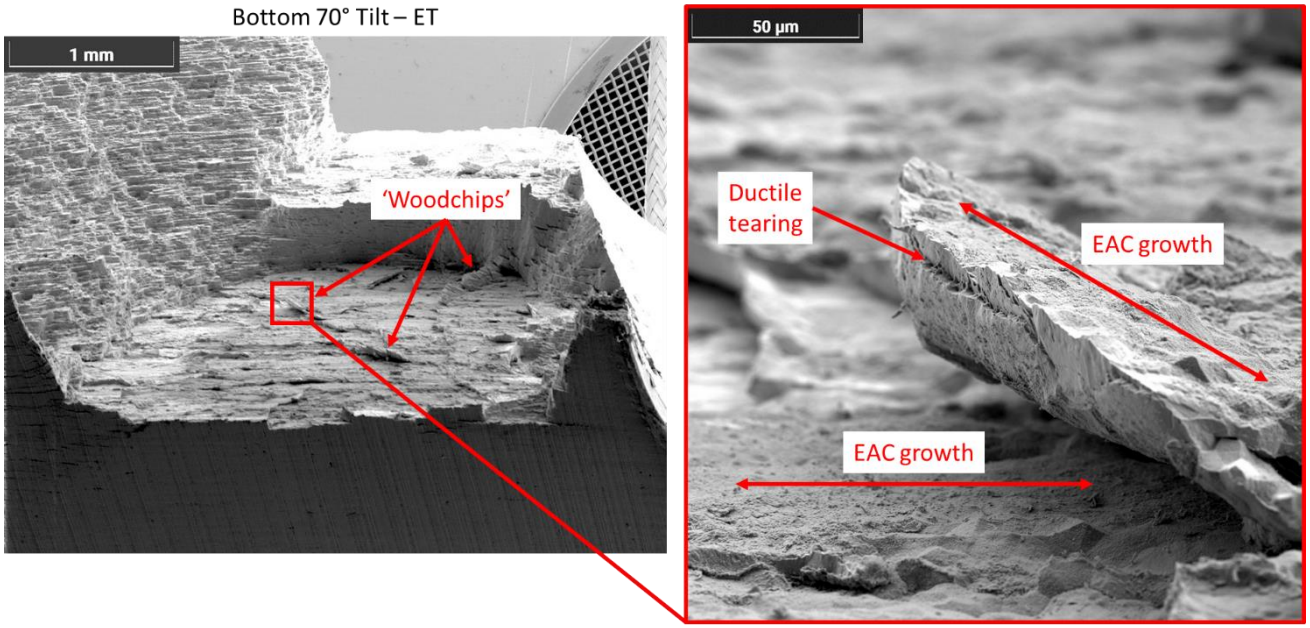


Figure 6 – High angle images of part of the coupon EAC crack showing the 'woodchip' features protruding from the crack surface. These features often exhibit ductile tearing around their edges.

Finally, the relative concentration of corrosion product across the aircraft and coupon crack surfaces can be compared to assess their comparative environments as well as the potential role that the corrosion may have in the growth process. This is particularly important when considering the relative roles of anodic dissolution and hydrogen embrittlement in the growth process. It was found that both the coupon and aircraft EAC cracks generally exhibited reducing corrosion product as the crack tips were approached. An example of this is shown for the coupon in Figure 7, where the expected growth directions are indicated with the black arrows, and a magnified view of the crack tip region is shown in the right image.

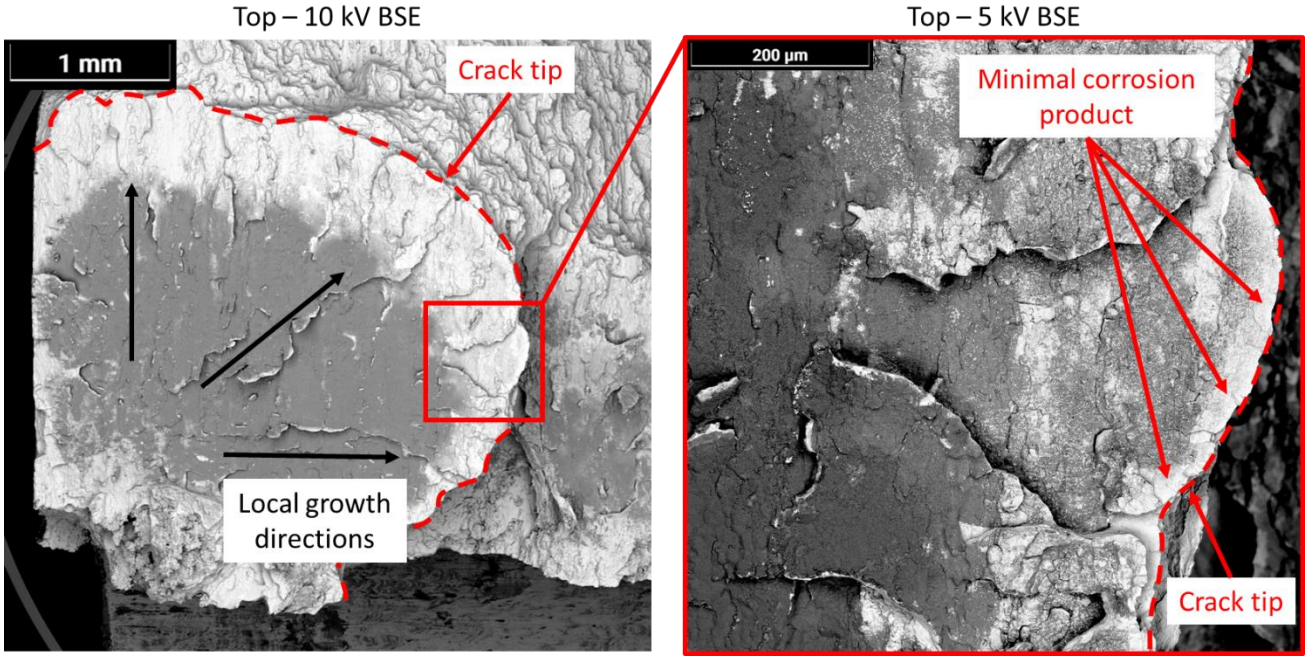


Figure 7 – BSE images of the coupon crack showing decreasing corrosion product as the crack tip is approached. The expected local crack growth directions are also indicated in the left image.

It is also worth noting that the right image in Figure 7 was taken at a lower acceleration voltage than the left image, and shows more evidence of the corrosion product on the surface. This is due to the corrosion product becoming increasingly thinner near the crack tip. Regardless, the lack of significant corrosion product right at the crack tip indicates that much of the corrosion occurred in the wake of the crack after it progressed beyond that point. This suggests that anodic dissolution at the crack tip may not have been a key mechanism of growth for the coupon or aircraft EAC, as there is a lack of corrosion product visible at the crack tip that would be associated with anodic dissolution.

3.3 Crack Arrest Marks

Beyond analysing the corrosion product on the crack surfaces, another feature that may provide clues as the mechanism of EAC growth is that of CAMs. Whilst CAMs are frequently mentioned in the literature [4, 11, 14, 15, 18, 20], there is still a lack of detailed analysis of matching CAM features, or a recognition of the varied appearance that these features can have. As such, this section will analyse a range of CAMs observed on both the coupon and aircraft cracks and assess what clues they may provide regarding the growth mechanism.

An example of a region of the coupon crack with evidence of CAMs is shown in Figure 8. This figure provides an image of both halves of the crack surface, named ‘top’ and ‘bottom’ for simplicity. CAMs can be seen to occur in matching locations across both halves, with some regions showing very similar features on the top and bottom (b), while others show quite dissimilar features (a). The nominal direction of growth for this region was from the bottom to the top of the image, whereas the CAMs can be seen to align in many different directions. This shows that the local direction of growth across a single grain facet may not align with the average growth direction of the crack, meaning that care should be taken when utilising CAM orientation to establish overall crack growth directions. Additionally, it can be seen that each grain facet typically either has CAMs evident across its entire

face on both fracture surfaces, or conversely has no evidence of CAMs on both fracture surfaces. This indicates that the production of CAMs may be related to the relative orientations of grain facets with their neighbors or the specific chemical composition between them, as the appearance is usually consistent across each complete facet.

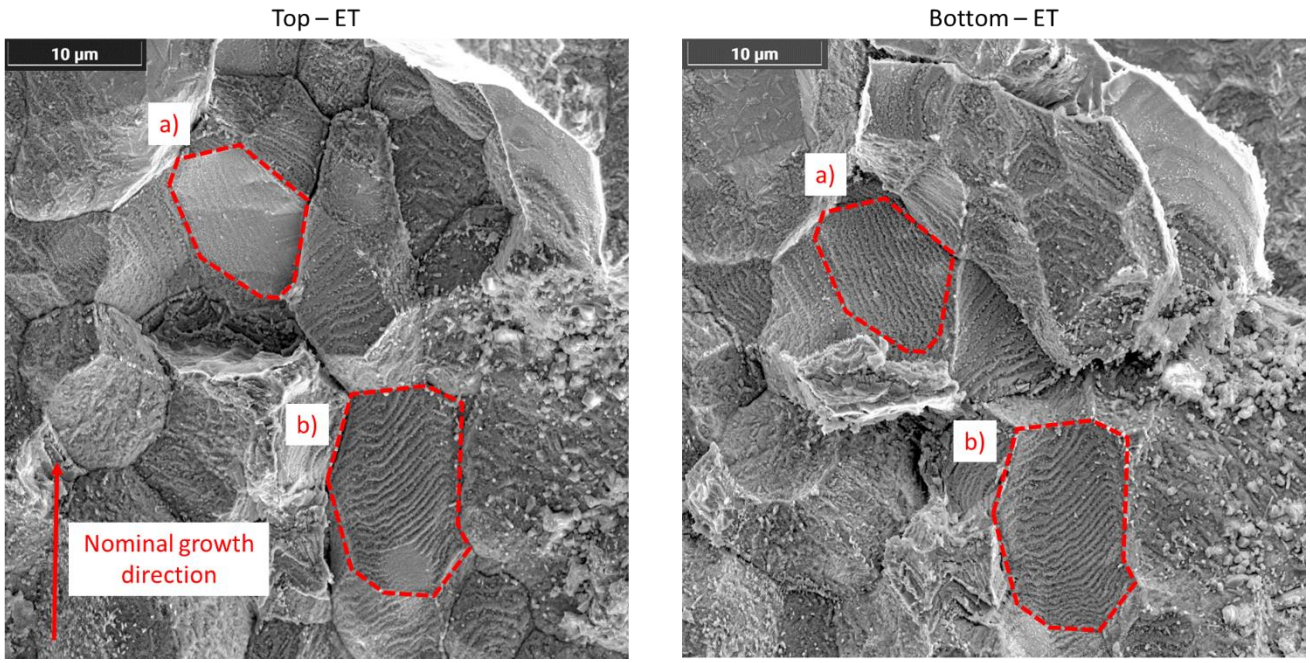


Figure 8 – An example of CAMs visible on matching crack faces. Region a) shows dissimilar features, while b) shows similar features.

A closer examination of facet b) in Figure 8 reveals CAMs similar to those discussed in the literature. Both halves of this region are shown in Figure 9, where each facet can be seen to contain multiple undulating ridge-valley features across their surfaces. These undulating features cover much of the aluminium alloy substrate and were found to be oxygen rich using EDS. It can be seen by tracing the ridges of these features, such as Figure 9a), that ridges match with ridges on the opposite crack face, creating a symmetric CAM appearance. This also indicates that there must be some small level of separation maintained between the crack faces for these CAMs to grow, as any considerable ridge-to-ridge contact would flatten them. It is also notable that some limited regions do not contain matching features, such as that shown in Figure 9b). Here, CAMs are visible on the bottom half, whilst not being evident in the same form on the top half. It is not clear why this abrupt and localised change occurs, but does suggest that the growth of CAMs is very sensitive to local environmental conditions and not dictated by the stress intensity factor, as the stress intensity factor was broadly consistent across this small region of growth.

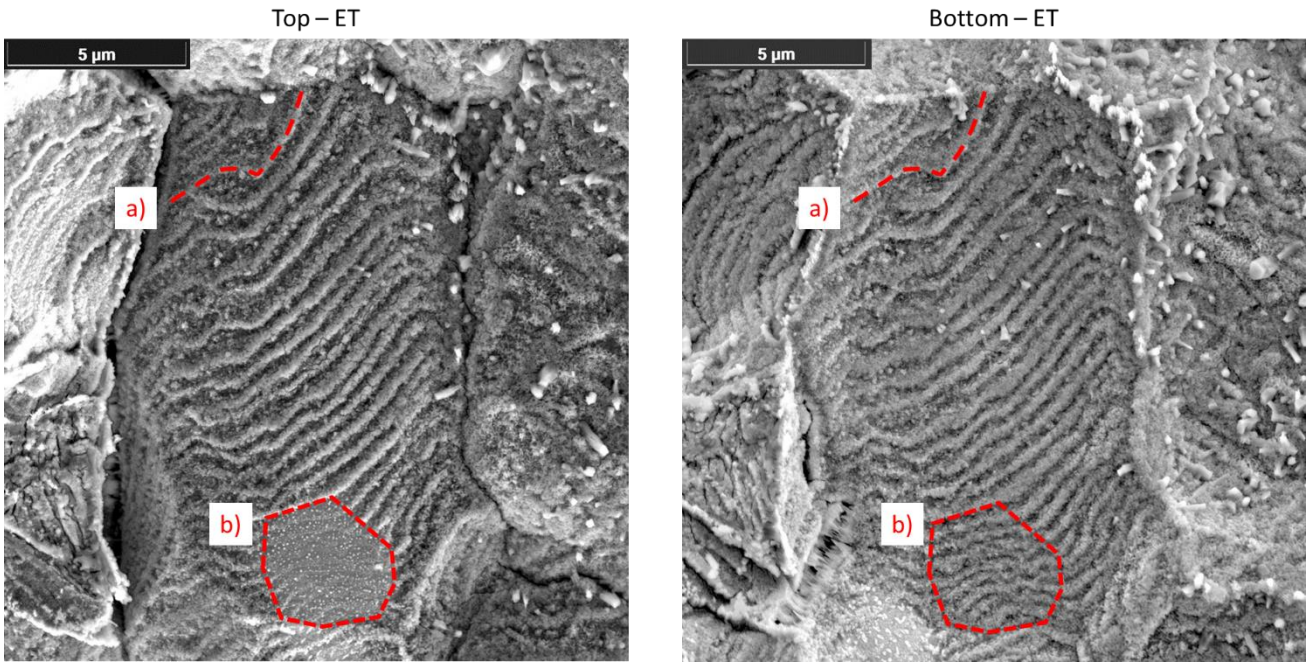


Figure 9 – A magnified image of the region shown in Figure 8b). Feature a) traces a single CAM along its length, showing how it matches on both halves. Feature b) shows a region where the top crack half appears relatively free of corrosion product compared to the bottom half.

Whilst CAMs produced by alternating increased oxide layer thickness were one of the more commonly observed forms observed on the pre-cleaned samples, there were also other features found with alternating patterns at spacings expected of CAMs. One example is that shown in Figure 10, which was taken with a BSE detector to provide composition contrast between the aluminium matrix and GBPs. This region shows alternating bands of increased GBP density followed by reduced GBP density, visible due to the GBPs appearing brighter than aluminium matrix when images using this detector. It does not, however, contain evidence of any major oxide layer buildup on the surface. Similar to the CAMs shown in Figure 8, the features in Figure 10 also have a relatively consistent appearance across full grain facets. To the authors' knowledge, the literature has not previously reported the appearance of CAMs such as these.

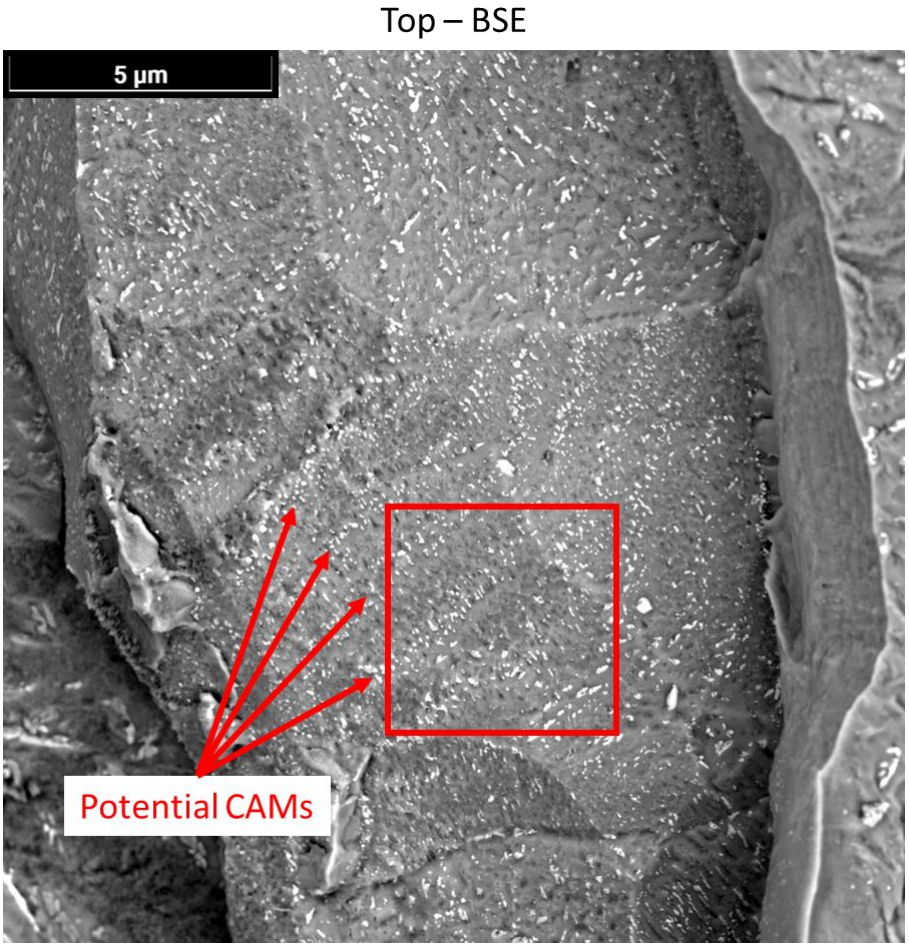


Figure 10 – BSE image of the crack showing alternative bands of higher GBP concentration. These bands are spaced at distances comparable to that expected for CAMs. The red box is further magnified in Figure 11.

Closer examination of the region bounded by the red box in Figure 10 is provided in Figure 11, including images of the matching location on the opposite crack surface. The GBP banding can be seen to occur on this matching bottom face, with regions of high and low GBP density mirroring each other. In the areas of high GBP density, some of the GBPs have been pulled from one surface, leaving behind matching voids consistent with particle pull out. An example of this is indicated in Figure 11, where three adjacent GBPs have been pulled from the top crack surface but remain embedded in the bottom surface.

The similarities between the alternating GBP bands and the alternating increased oxide layer thickness support the idea that both may be different forms of CAMs. Both suggest that there may be regions of alternating increased chemical activity, with one form growing an increased oxide layer while the other experiences increased GBP dissolution. This second form of CAMs provides evidence that dissolution of GBPs may be an important mechanism associated with EAC growth. However, it is worth mentioning that whilst this GBP banding was observed in more than just the location shown here, the majority of the EAC surfaces showed no such evidence, indicating that this behaviour may be dictated by very specific local conditions. In the regions where this GBP dissolution did occur it supports them being anodic, while the aluminium is likely cathodic. Additionally, the absence of significant plastic deformation around GBP pull out sites indicates that crack growth did not proceed by ductile tearing. Rather, the fracture morphology was quasi-brittle and consistent with hydrogen embrittlement, with any contribution from anodic dissolution of GBPs likely mechanistically coupled to hydrogen embrittlement in enabling crack propagation

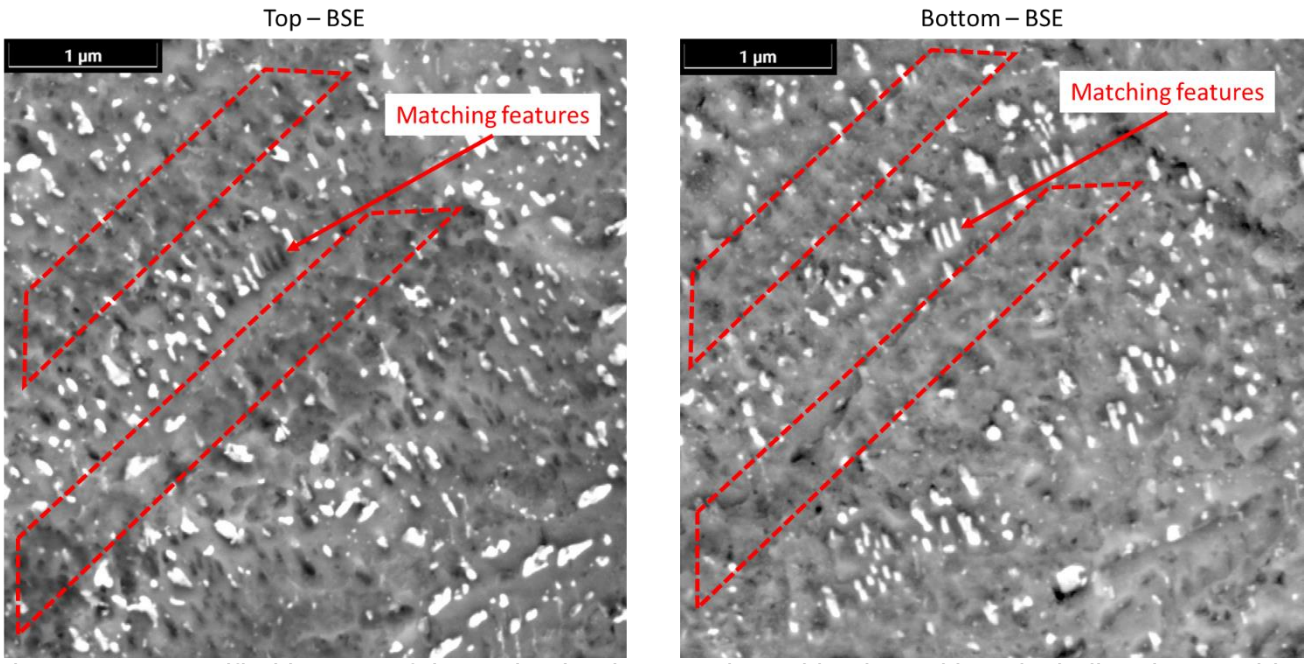


Figure 11 – Magnified images of the region in Figure 10 bound by the red box, including the matching top surface crack face. Alternate bands of GBPs can be seen on both crack surface halves.

It's also worthwhile considering whether CAMs develop in their entirety prior to the crack tip stepping forwards, or whether chemical activity continues behind each crack tip preferentially in these locations well after it has passed these points. This could lead to the continued growth of oxide or corrosion and dissolution of GBPs behind the crack tip. One observation related to this is the increasing corrosion product near the initiation location of most coupon and aircraft EAC cracks, as was discussed relating to Figure 7. This suggests that the corrosion product may continue to grow on the surface behind the crack tip. If this is true, it may result in CAMs being less visible near the tip compared to sufficiently far behind it where the corrosion product thickness has had more time to fully develop.

Based on the above observation, as well as the known increased surface sensitivity using reduced FEGSEM acceleration voltages, some of the coupon and aircraft cracks were analysed using a 0.5 kV acceleration voltage and an in-lens detector designed for use with such low voltages. An image taken with these settings compared to one taken with a 5 kV acceleration voltage and ET detector is shown in Figure 12. CAMs can be seen using the 0.5 kV acceleration voltage, while they are not evident with the 5 kV acceleration voltage, indicating that the CAMs are very thin in this location. Additionally, some localised regions of thicker corrosion product can be observed adjacent to the CAMs. These regions have multiple cracks running through them, some of which can be seen to directly align with adjacent CAMs. This suggests that the cracking in the corrosion product was not random, rather that these regions may have had local environments that allowed the rapid growth of the CAMs into larger features in a systematic manner. It is apparent, then, that the oxide layer associated with CAMs likely does grow over time behind the crack tip, and means that CAMs will be harder to observe near the crack tip. This is one possible explanation why some research has only identified CAMs near the crack initiation locations [14, 15], though there is still a possibility that no CAMs would be visible regardless.

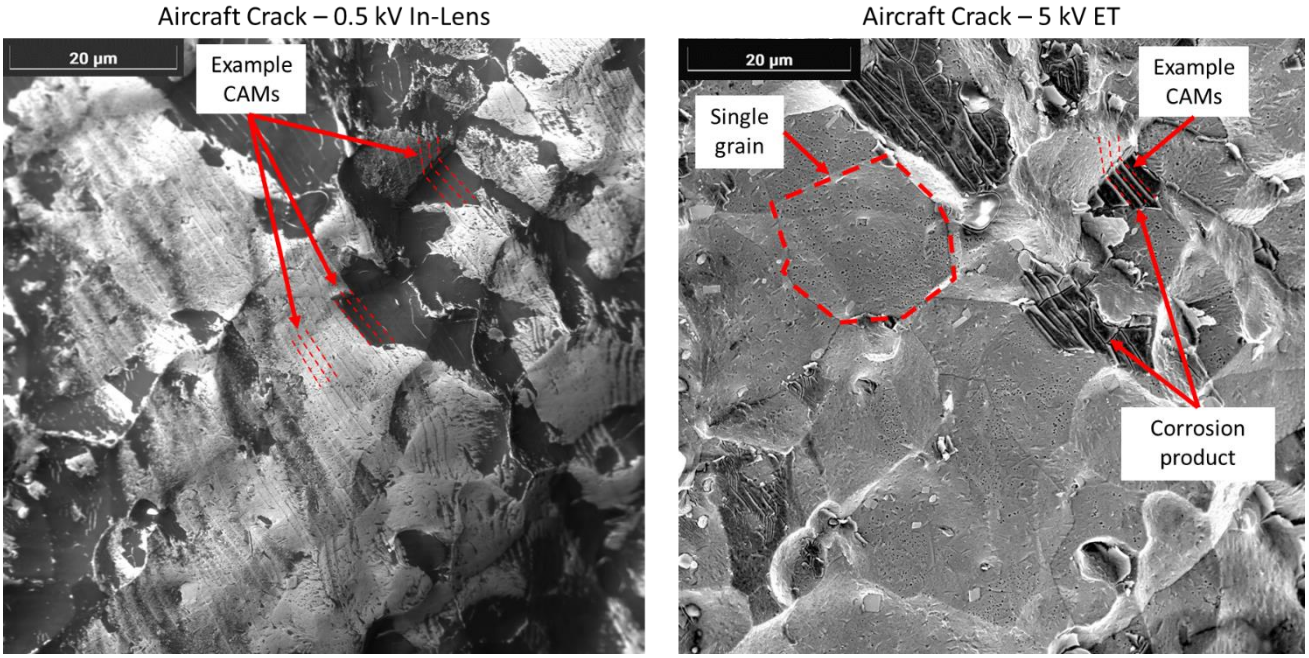


Figure 12 – Two FEGSEM images of an aircraft EAC crack in the same location using different settings. The image on the left shows CAMs where the settings used in the right image do not.

Another question that remains is whether CAMs are observable after cleaning, particularly those related to increased oxide layer thickness. This is because there is debate in the literature as to whether CAMs are produced only through a chemical process, or whether there is underlying physical deformation. As such, an example of the top surface CAMs in Figure 9 are shown both pre-cleaning and post-cleaning in Figure 13. The cleaning was done in accordance with ASTM G1 process C.1.1 [34], which is designed to minimise removal of the substrate material whilst cleaning off any corrosion product. This lack of damage to the base metal appears to be confirmed through the similar appearance of region b) before and after cleaning. However, the possibility of localised attack associated with regions of the CAMs should be acknowledged, and would require further analysis outside the scope of this paper. The CAM pattern observed after cleaning matches that prior to cleaning, with the ridges matching in both cases, as shown by feature a). However, the valleys appear to be made up of multiple adjacent small corrosion pits, suggesting the anodic dissolution of the material in these regions. It is likely, then, that the ridges of the CAMs prior to cleaning were accentuated by the buildup of corrosion debris adjacent to the pits. These CAMs appear to be produced through chemical processes, rather than any clear degree of plastic deformation. This is, however, only one example, and a range of other locations would need to be analysed in detail prior to considering this as the standard behaviour.

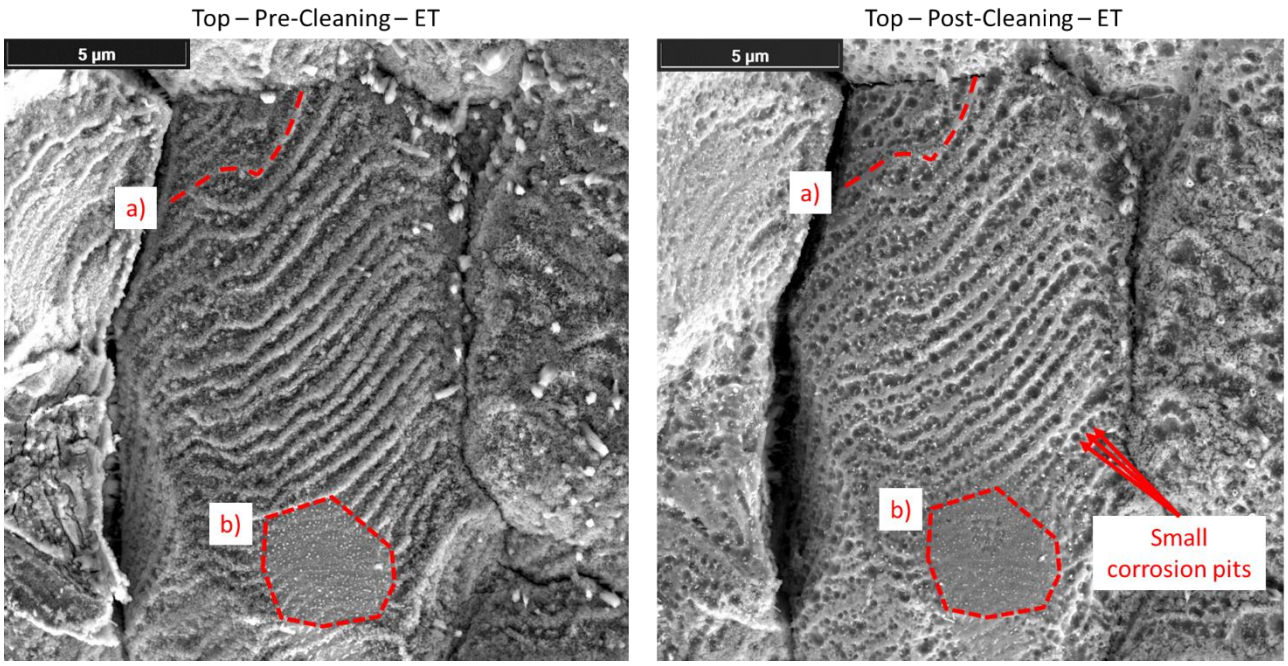


Figure 13 - An example of the top surface CAMs shown in Figure 9 both pre-cleaning and post-cleaning. Many of the same features can be observed, where the CAMs are still clearly visible even after cleaning off the corrosion product in accordance with ASTM G1 process C.1.1.

Finally, whilst the literature often quotes CAMs as having fairly consistent average spacing for each material [26], there has been little work expanding on what the typical variation in spacing might be, or in what locations the spacing may change. As such, examples of two grain facets with different CAM spacings located near each other are provided in Figure 14 and Figure 15. These two facets were chosen qualitatively based on the visually observable significant difference in their CAM spacings. It's worth noting that individual grain facets would generally maintain self-similar spacing, but that the spacing could be vastly different between nearby facets. This is consistent with the observation that CAMs generally appear across an entire facet or not on any part of the facet, suggesting that the growth process is constant across any individual facet.

The average CAM spacing in Figure 14 is 340 nm, while it is 775 nm in Figure 15. The lower of these values is within the bounds of what has been quoted in the literature, though the upper value is outside of the typical spacing [11, 16, 26]. This variability shows that citing any single value for CAM spacing for a material may obscure the underlying variability and complexity. What this variability in close proximity does show is that the stress intensity factor appears to be a far less important factor associated with CAM spacing than other local chemical and physical factors.

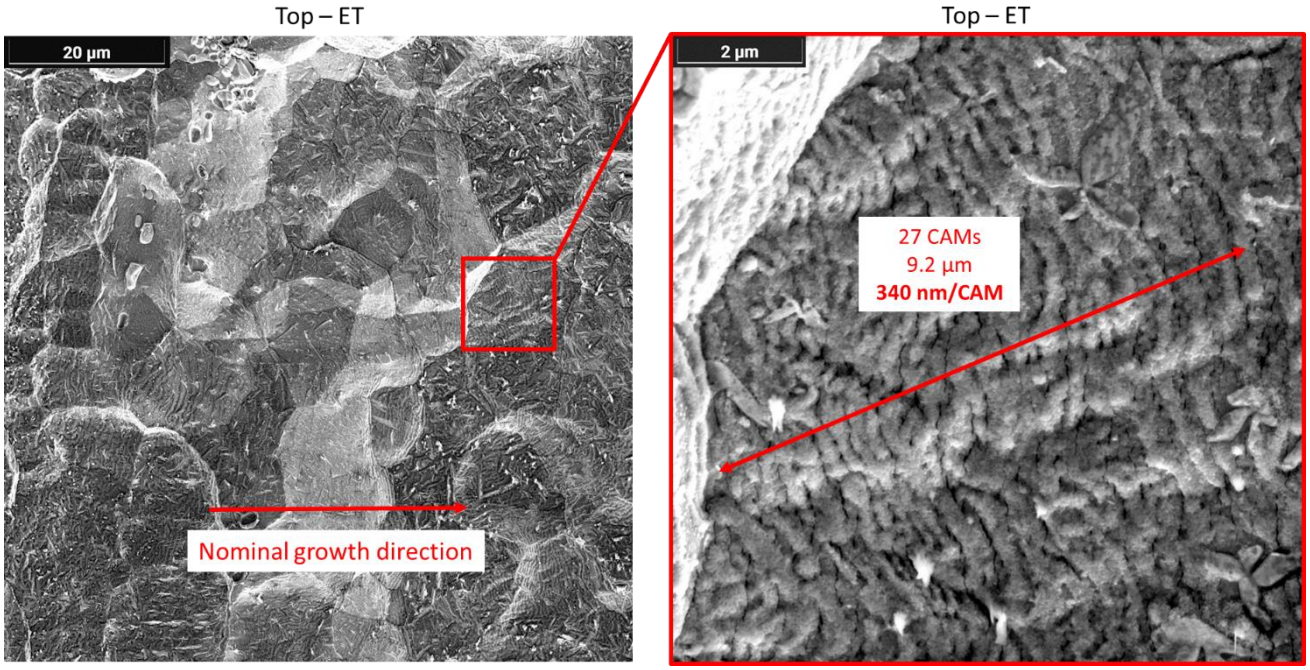


Figure 14 – An image showing a grain facet with CAMs as well as their measured average spacing. This spacing can be compared to Figure 15, which is located nearby.

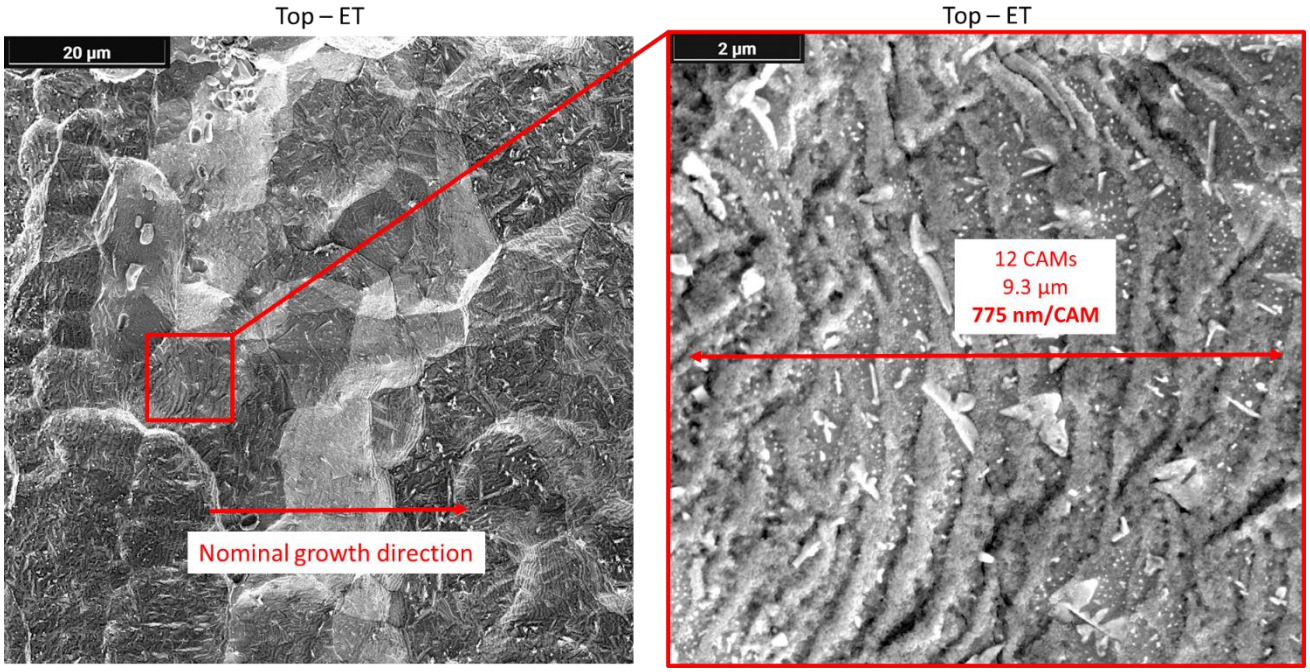


Figure 15 - An image showing a grain facet with CAMs as well as their measured average spacing. This spacing can be compared to Figure 14, which is located nearby.

3.4 River Patterns

As was mentioned in section 3.2, most of the EAC cracks exhibited 'woodchip' features on the surface associated with secondary cracking and tearing between different planes of growth. It is worth considering whether these features can be used similar to river patterns in fatigue [27-29], allowing them to be rapidly traced back to near where the crack initiated from. Examples of some of these potential features are shown in Figure 16, which shows the same crack surface at two different angles. The features c) and d) are the two most prominent and continuous of these features, while a), b), and d) are all significantly smaller. It's additionally worth noting that features a) and e) are aligned with the longitudinal grain direction, meaning that they could simply be associated with the elongated packets of similarly orientated grains.

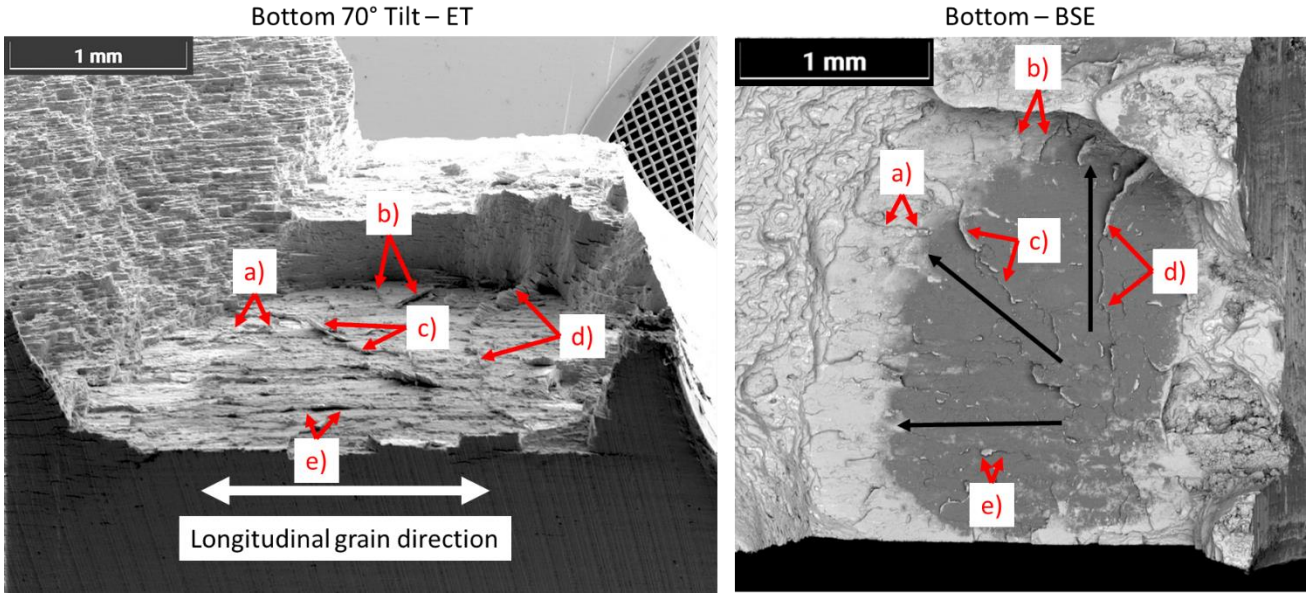


Figure 16 - Examples of some of the more clearly visible features on the coupon crack surface that could be considered similar to river patterns. Both images are of the same crack, but the left image is tilted 70°. The expected local growth directions based on these features are indicated with the black arrows, and the longitudinal grain direction is marked by the white arrow.

Closer examination of each of the features in Figure 16 revealed a pattern associated with the appearance of their edges. For the smaller features aligned with the longitudinal grain direction, their edges were predominantly intergranular EAC, including some regions with visible CAMs, such as is shown in Figure 17 for feature a). In contrast, many of the features aligned at an angle to the longitudinal grain direction had edges that predominantly exhibited evidence of ductile tearing. This tearing most likely occurred post-testing when overloading the crack to separate its two halves. The presence of the ductile tearing shows that the crack had not crossed this boundary from either side during the EAC growth, and hence must have been growing parallel to it, at least in the region local to that feature. This suggests that these features can be considered analogous to river patterns in fatigue provided they failed through ductile tearing, rather than EAC growth. It appears that the features aligned with the longitudinal grain direction are the most likely to have grown due to EAC, though features should be considered on a case-by-case basis. Regardless, these features may be useful in tracing EAC cracks back to their initiating locations. In this case, the ‘river patterns’ agree with the aforementioned expected initiation at the PP+AC pit near the corner of the crack.

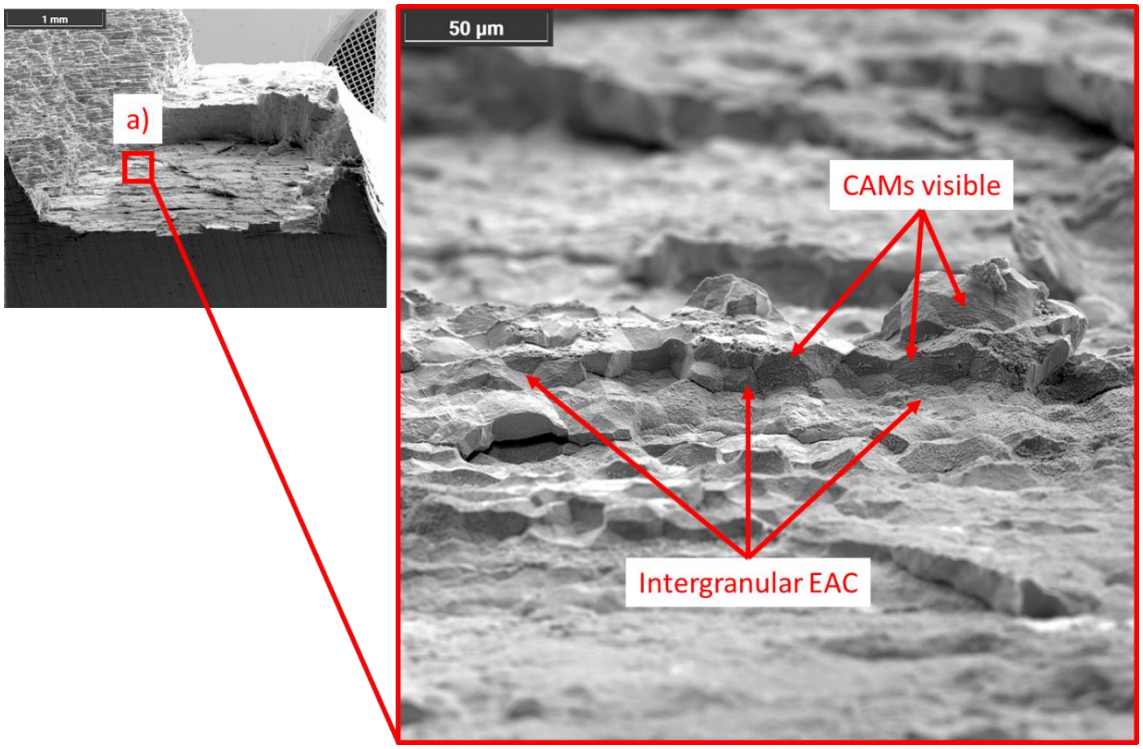


Figure 17 - An example of feature a) from Figure 16, where its edges are predominantly intergranular EAC, including CAMs being visible on some facets.

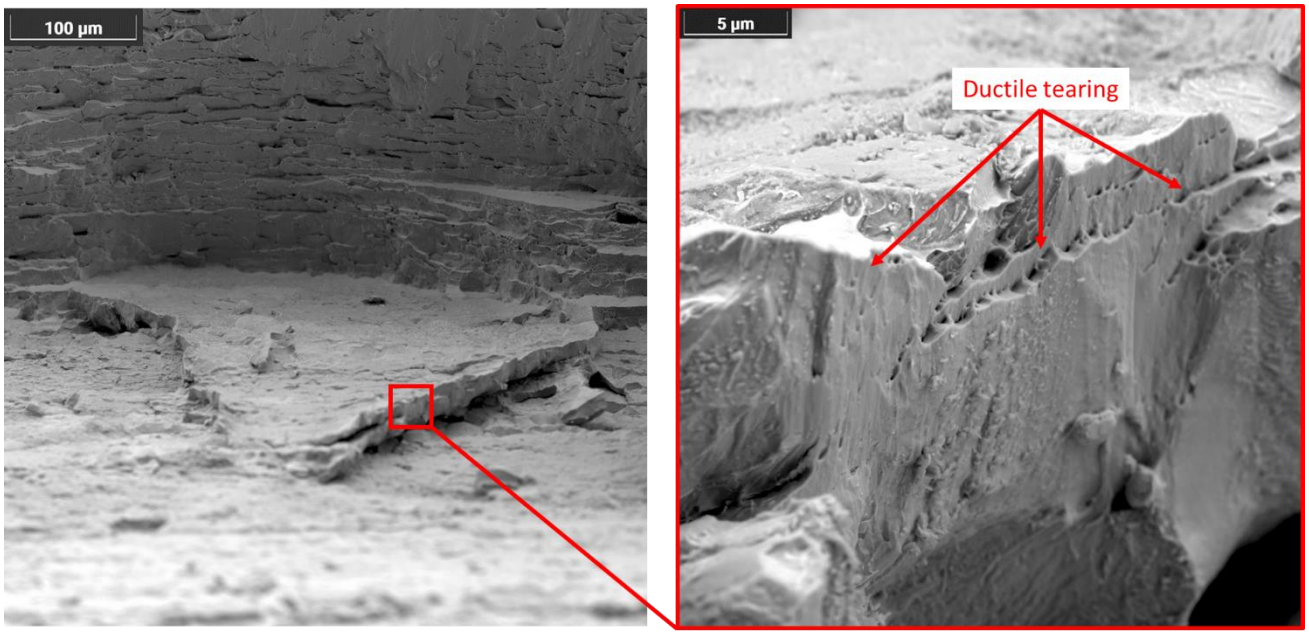


Figure 18 - An example of feature b) from Figure 16, where its edges predominantly exhibit evidence of ductile tearing.

4. Conclusions

This paper provided multiple fractographic images from both coupon and aircraft EAC cracks, focusing on prominent features that may provide clues as to how they grew. This included analysing the variation in appearance of EAC cracks depending on the choice of FEGSEM acceleration voltage and detector, where it was found that lower acceleration voltages were generally better for observing features such as CAMs. It was also found that a thin layer of corrosion product was evident over much of the crack surfaces, with reducing concentration near the crack tips. This indicates that the corrosion process was ongoing well after the crack tip had passed beyond each region. Similarly, the oxide layer thickness associated with CAMs appears to have increased over time after the crack tip had passed beyond them, suggesting that they are less likely to be observed near the crack tip before they have increased sufficiently in thickness. The spacing of CAMs also varied significantly between grain facets located very near each other, showing that variables other than the stress intensity factor

dictate this spacing. Finally, out-of-plane features akin to fatigue crack river patterns were analysed, where it was found that many of them did align with the local direction of crack growth. This means that these features could be used in the future to trace EAC cracks back to near where they initiated.

Acknowledgements

The authors would like to acknowledge Maria Salagaras for being instrumental in the development of the PP+AC solution, and Ben Dixon for his guidance and support through this work.

References

[1] T. Prabhu, "An Overview of High-Performance Aircraft Structural Al Alloy-AA7085," *Acta Metallurgica Sinica (English Letters),* vol. 28, 05/03 2015, doi: 10.1007/s40195-015-0275-z.
[2] B. Main, B. Dixon, M. Jones, and S. Barter, "Microstructure and surface finish influences on AA7085-T7452 small fatigue crack growth rates," *Engineering Failure Analysis,* vol. 141, p. 106628, 2022/11/01/ 2022, doi: https://doi.org/10.1016/j.engfailanal.2022.106628.
[3] L. Mueller, L. Suffredini, D. Bush, R. Sawtell, and P. Brouwer, "Alcoa Green Letter - Alcoa 7085 Die Forgings, 7th Generation Structural Solutions, 3rd Edition," 2006.
[4] E. Schwarzenböck *et al.*, "Environmental cracking performance of new generation thick plate 7000-T7x series alloys in humid air," *Corrosion Science,* vol. 171, p. 108701, 2020/07/15/ 2020, doi: https://doi.org/10.1016/j.corsci.2020.108701.
[5] B. Main, M. Jones, B. Dixon, and S. Barter, "On small fatigue crack growth rates in AA7085-T7452," *International Journal of Fatigue,* vol. 156, p. 106704, 2022/03/01/ 2022, doi: https://doi.org/10.1016/j.ijfatigue.2021.106704.
[6] EASA, "Environmentally Assisted Cracking in certain Aluminium Alloys," 2021, vol. 2018-04R2.
[7] *Standard Practice for Exposure of Metals and Alloys by Alternate Immersion in Neutral 3.5 % Sodium Chloride Solution*, G44-21, ASTM, 2021.
[8] C. Dalle Donne, "Structural Integrity - The Journey Towards Zero Emission Commercial Aircraft," in *International Committee on Aeronautical Fatigue*, Delft, 26-29 June 2023.
[9] L. Christodoulou and H. M. Flower, "Hydrogen embrittlement and trapping in Al6%·Zn-3%·Mg," *Acta Metallurgica,* vol. 28, no. 4, pp. 481-487, 1980/04/01/ 1980, doi: https://doi.org/10.1016/0001-6160(80)90138-8.
[10] L. Oger, E. Andrieu, G. Odemer, L. Peguet, and C. Blanc, "About the role of the hydrogen during stress corrosion cracking of a low-copper Al-Zn-Mg alloy," *Journal of Alloys and Compounds,* vol. 900, p. 163391, 2022/04/15/ 2022, doi: https://doi.org/10.1016/j.jallcom.2021.163391.
[11] N. J. H. Holroyd and G. M. Scamans, "Crack Propagation During Sustained-Load Cracking of Al-Zn-Mg-Cu Aluminum Alloys Exposed to Moist Air or Distilled Water," *Metallurgical and Materials Transactions A,* vol. 42, pp. 3979-3998, 12/01 2011, doi: 10.1007/s11661-011-0793-x.
[12] M. López Freixes *et al.*, "Revisiting stress-corrosion cracking and hydrogen embrittlement in 7xxx-Al alloys at the near-atomic-scale," *Nature Communications,* vol. 13, no. 1, p. 4290, 2022/07/25 2022, doi: 10.1038/s41467-022-31964-3.
[13] Y. Yang, Y. Wu, S. Jin, D. Wang, S. Zhang, and M. Zha, "A brief review on stress corrosion cracking of aluminum alloys: Mechanisms, prevention, and future perspectives," *Journal of Alloys and Compounds,* vol. 1037, p. 182430, 2025/08/10/ 2025, doi: https://doi.org/10.1016/j.jallcom.2025.182430.
[14] Y. Aboura *et al.*, "Understanding the environmentally assisted cracking (EAC) initiation and propagation of new generation 7xxx alloys using slow strain rate testing," *Corrosion Science,* vol. 199, p. 110161, 2022/05/01/ 2022, doi: https://doi.org/10.1016/j.corsci.2022.110161.
[15] R. T. Euesden *et al.*, "In-situ observation of environmentally assisted crack initiation and short crack growth behaviour of new-generation 7xxx series alloys in humid air," *Corrosion Science,* vol. 216, p. 111051, 2023/05/15/ 2023, doi: https://doi.org/10.1016/j.corsci.2023.111051.
[16] N. J. H. Holroyd and G. M. Scamans, "Stress Corrosion Cracking in Al-Zn-Mg-Cu Aluminum Alloys in Saline Environments," *Metallurgical and Materials Transactions A,* vol. 44, no. 3, pp. 1230-1253, 2013/03/01 2013, doi: 10.1007/s11661-012-1528-3.
[17] S. P. Lynch, "Mechanisms of stress-corrosion cracking and liquid-metal embrittlement in Al-Zn-Mg bicrystals," *Journal of Materials Science,* vol. 20, no. 9, pp. 3329-3338, 1985/09/01 1985, doi: 10.1007/BF00545203.
[18] G. Young, *Hydrogen Production, Absorption, and Transport During Environment Assisted Cracking of an Al-Zn-Mg-(Cu) Alloy in Humid Air*. 2003.
[19] R. Ricker, E. Lee, R. Taylor, C. Lei, B. Pregger, and E. Lipnickas, "Chloride Ion Activity and Susceptibility of Al Alloys 7075-T6 and 5083-H131 to Stress Corrosion Cracking," *Metallurgical and Materials Transactions A,* vol. 44A, pp. 1353-1364, 03/01 2013, doi: 10.1007/s11661-012-1500-2.
[20] S. Lynch, "A review of underlying reasons for intergranular cracking for a variety of failure modes and materials and examples of case histories," *Engineering Failure Analysis,* vol. 100, 02/01 2019, doi:

10.1016/j.engfailanal.2019.02.027.
[21] N. J. H. Holroyd, T. Burnett, J. Lewandowski, and G. M. Scamans, "Environment-Induced Cracking of High-Strength Al-Zn-Mg-Cu Aluminum Alloys: Past, Present, and Future," *Corrosion,* vol. 79, pp. 48-71, 10/27 2022, doi: 10.5006/4149.
[22] J. Srivastava *et al.*, "The influence of partially recrystallized grain structures on hydrogen-environmentally induced cracking (H-EIC) behavior of AA7085 alloy in humid air," *Corrosion Science,* vol. 256, p. 113199, 2025/11/01/ 2025, doi: https://doi.org/10.1016/j.corsci.2025.113199.
[23] R. T. Euesden *et al.*, "Direct comparison of the environmentally induced cracking resistance of 2nd and 3rd generation alloys, AA7050-T7651 and AA7085-T7651," *Materials & Design,* vol. 253, p. 113867, 2025/05/01/ 2025, doi: https://doi.org/10.1016/j.matdes.2025.113867.
[24] S. Lynch, "Some fractographic contributions to understanding fatigue crack growth," *International Journal of Fatigue,* vol. 104, pp. 12-26, 2017/11/01/ 2017, doi: https://doi.org/10.1016/j.ijfatigue.2017.06.036.
[25] C. R. Brooks and B. L. McGill, "The application of scanning electron microscopy to fractography," *Materials Characterization,* vol. 33, no. 3, pp. 195-243, 1994/10/01/ 1994, doi: https://doi.org/10.1016/1044-5803(94)90045-0.
[26] S. Knight, "Stress Corrosion Cracking of Al-Zn-Mg-Cu Alloys," Doctor of Philisophy, Department of Materials Engineering, Monash University, 2008.
[27] I. Field, E. Kandare, J. Tian, and S. Barter, "Use of the helium ion microscope in small crack fractography," *Engineering Failure Analysis,* vol. 139, p. 106483, 2022/09/01/ 2022, doi: https://doi.org/10.1016/j.engfailanal.2022.106483.
[28] I. Field, B. Dixon, E. Kandare, J. Tian, and S. Barter, "The relationship between surface roughness and fatigue crack growth rate in AA7050-T7451 subjected to periodic underloads," *International Journal of Fatigue,* vol. 167, p. 107355, 2023/02/01/ 2023, doi: https://doi.org/10.1016/j.ijfatigue.2022.107355.
[29] A. Deschamps, S. Péron, Y. Bréchet, J. C. Ehrström, and L. Poizat, "High temperature, high strain rate embrittlement of Al-Mg-Mn alloy: evidence of cleavage of an fcc alloy," *Materials Science and Technology,* vol. 18, no. 10, pp. 1085-1091, 2002/10/01 2002, doi: 10.1179/026708302225005972.
[30] B. Main, L. Jiang, R. K. W. Marceau, and S. Barter, "Material characterisation of anodising effects on small fatigue crack initiation in AA7XXX alloys," *Materialia,* vol. 33, p. 101997, 12/01 2023, doi: 10.1016/j.mtla.2023.101997.
[31] A. C. U. Rao, V. Vasu, M. Govindaraju, and K. V. S. Srinadh, "Stress corrosion cracking behaviour of 7xxx aluminum alloys: A literature review," *Transactions of Nonferrous Metals Society of China,* vol. 26, no. 6, pp. 1447-1471, 2016/06/01/ 2016, doi: https://doi.org/10.1016/S1003-6326(16)64220-6.
[32] R. Hill, J. Notte, and B. Ward, "The ALIS He ion source and its application to high resolution microscopy," *Physics Procedia,* vol. 1, no. 1, pp. 135-141, 2008/08/01/ 2008, doi: https://doi.org/10.1016/j.phpro.2008.07.088.
[33] Y. Yang, A. Kushima, W. Han, H. Xin, and J. Li, "Liquid-Like, Self-Healing Aluminum Oxide during Deformation at Room Temperature," *Nano Letters,* vol. 18, no. 4, pp. 2492-2497, 2018/04/11 2018, doi: 10.1021/acs.nanolett.8b00068.
[34] *Standard Practice for Preparing, Cleaning, and Evaluating Corrosion Test Specimens*, G1-90, ASTM, 1999.

Copyright Statement

The authors confirm that they, and/or their company or organization, hold copyright on all of the original material included in this paper. The authors also confirm that they have obtained permission, from the copyright holder of any third party material included in this paper, to publish it as part of their paper. The authors confirm that they give permission, or have obtained permission from the copyright holder of this paper, for the publication and distribution of this paper as part of the ICAS proceedings or as individual off-prints from the proceedings.